Food Chemistry: X 19 (2023) 100784

Contents lists available at ScienceDirect

Food Chemistry: X

journal homepage: www.sciencedirect.com/journal/food-chemistry-x

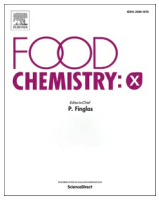

# Structural analysis, nutritional evaluation, and flavor characterization of parched rice made from proso millet

Yulian Zhu [a,1], Fei Xie [a,1], Jing Ren [a], Fan Jiang [a], Ning Zhao [a], Shuang-kui Du [a,b,c,*]

[a] College of Food Science and Engineering, Northwest A & F University, Yangling 712100, China
[b] Engineering Research Center of Grain and Oil Functionalized Processing, Yangling, Shaanxi 712100, China
[c] Shaanxi Union Research Center of University and Enterprise for Grain Processing Technologies, Yangling, Shaanxi 712100, China

ARTICLE INFO

*Keywords:*
Proso millet
Structural analysis
Nutritional value
Volatile compound

ABSTRACT

This study investigated the structure and quality characteristics of hard and crispy parched rice obtained from raw proso millet through steaming, roasting, and milling. Results showed that thermal treatment disrupted the structure of samples and transformed the crystal from A-type in raw proso to V-type in parched rice. Rheological and thermodynamic analyses revealed that thermal treatment reduced the stability of parched rice. Gelatinization tests demonstrated that the parched rice was easier to gelatinize and had a lower viscosity. The digestibility of hard parched rice and crispy parched rice improved, with rapidly digestible starch content increasing by 73.62% and 76.95%, respectively, compared with that of raw proso millet. Headspace solid-phase microextraction/gas chromatography-mass spectrometry results further indicated that thermal treatment enhanced the flavor substances of parched rice. These findings demonstrated the unique properties of parched rice and supported its production and processing as a whole grain.

## 1. Introduction

Proso millet (*Panicum miliaceum* L.) is an annual herbaceous plant in family Poaceae, that is widely grown in subtropical regions of Asia, Europe, and China. It has a high photosynthesis capacity and can withstand cold and drought (Marti & Tyl, 2021). As a traditional grain, proso millet is rich in nutrients and bioactive substances such as starch, protein, essential minerals, unsaturated fatty acids, and phenolic compounds (Saleh, Zhang, Chen, & Shen, 2013). Proso millet is a gluten-free grain with numerous potential applications in human nutrition and food safety (Marti & Tyl, 2021; McSweeney, Seetharaman, Ramdath, & Duizer, 2017). However, the lack of refinement and processing limits its extensive use and acceptability. Proso millet has also recently drawn increased attention for its unique benefits to human health, but the processing technology and quality evaluation of related traditional products are less studied (Kumar, Sadiq, & Anal, 2020).

Thermal treatment is one of the most common grain-processing maturation methods and is extensively utilized in the food industry due to its safety and stability. During thermal treatment, a series of physicochemical changes, such as starch pasting, protein denaturation, and browning reactions may occur in the nutritional components of grains (Kumar et al., 2020). These changes may affect grains' sensory, structural properties, and nutritional qualities. Roasting, steaming, stir frying, and extrusion are commonly used in the thermal treatment of grains. Apart from the advantage of simple processes, they also impart unique toasted, grassy, and fruity flavors to the grains (Liu, Tang, & Zhang, 2012). Headspace solid-phase microextraction (HS-SPME)/gas chromatography (GC)-mass spectrometry (MS) and electronic nose (e-nose) analyses are primarily used to explore volatile substances in foods and are extensively used in food processing (Cai, Zhu, Ma, Thakur, Zhang, & Wei, 2020).

Parched rice, is a traditional whole grain favored by Inner Mongolians. It is usually prepared from proso millet through steaming, roasting, and milling processes. It is portable, easy to eat, and nutrient rich, making it a crucial part of most people's daily diets. The thermal treatment induces many physical and chemical changes in the nutritional components of cereal grains during processing, imparting unique edible quality and nutritional properties to them (Qian, Sun, Zhu, Zhang, Tian, & Wang, 2020). Roasting also imparts a special aroma to the sample. The unique aroma and flavor of parched rice are also reasons

* Correspondence author at: College of Food Science and Engineering, Northwest A & F University, Yangling 712100, China.
*E-mail addresses:* pinellia1999@163.com (Y. Zhu), CC19902431@163.com (F. Xie), renjingym@163.com (J. Ren), jiangfan9592@163.com (F. Jiang), 874594368@qq.com (N. Zhao), dushuangkui@nwafu.edu.cn (S.-k. Du).
[1] These authors contributed equally to this work.

https://doi.org/10.1016/j.fochx.2023.100784
Received 7 February 2023; Received in revised form 24 June 2023; Accepted 3 July 2023
Available online 4 July 2023

for its popularity among consumers. Many factors influence the nutritional values and quality properties of cooked grain, such as cooking time, method, and temperature (Starr, Bredie, & Hansen, 2013; Srikaeo, Furst, Hosken, & Ashton, 2005). Therefore, studying the quality characteristics of proso millet parched rice made from different methods is necessary.

The present study aimed to treat different varieties of proso millets with various methods and subsequently evaluate the nutritional values and volatile compounds of the different parched rice obtained. Findings in this study will guide the industrial processing and quality evaluation of parched rice as a whole grain.

## 2. Materials and methods

### 2.1. Materials

White proso millet, yellow proso millet, and red proso millet were provided by Fugu County (Yulin, Shaanxi, China). The α-amylase, glucosidase, rutinum, and gallic acid were purchased from Sigma-Aldrich Co. (St. Louis, USA). Other reagents and solvents were all of the analytical grades.

### 2.2. Preparation of parched rice

The preparation of parched rice is shown in Fig. 1, and the specific method was as follows. Depending on the variations, the proso millets were cooked in boiling water for varied amounts of time (white proso millet 40 min, yellow proso millet 60 min, red proso millet 70 min). Following treatment, samples were drained and promptly roasted at 220 °C for 3 min, and then milled to obtain hard parched rice (white hard parched rice WHPR, yellow hard parched rice YHPR, red hard parched rice RHPR). The proso millets were steamed in boiling water for 30 min, drained and quickly roasted at 250 °C for 2 min. Samples were cooled down and milled to obtain crispy parched rice (white crisp parched rice WCPR, yellow crisp parched rice YCPR, red crisp parched rice RCPR). The proso millets were milled to obtain raw proso millet (white proso millet WPM, yellow proso millet YPM, and red proso millet RPM). All samples were ground, passed through a 60-mesh sieve, and kept dry.

### 2.3. Determination of proximate composition

The moisture, protein, lipid, and ash contents of samples were measured according to the Association of Official Analysis Chemists' methods (AOAC, 2005). Total starch content was determined using the assay kits (Megazyme International Ireland Ltd., Ireland) following the manufacturer's instructions. Amylose content was investigated using the iodine colorimetric determination method of Jiang, Du, Guo, Fu, Jiang, and Du (2020).

### 2.4. Structure characterization

#### 2.4.1. Scanning electron microscopy

The surface morphology of samples was observed on a scanning electron microscope (SEM S-3400N, Hitachi, Tokyo, Japan). The sample was attached to the sample stage, and metalized with gold using a sputter coater. Images were collected at 8000 × .

#### 2.4.2. X-ray diffraction

According to the previous study by Li, Wen, Chen, Zhang, and Guo (2021) with slight modifications, an X-ray diffractometer (XRD D8 ADVANCE A25, Bruker, Germany) was used at the operating voltage of 40 kV and current of 20 mA, scanning from 4° to 45° with an angle step of 0.1°/s.

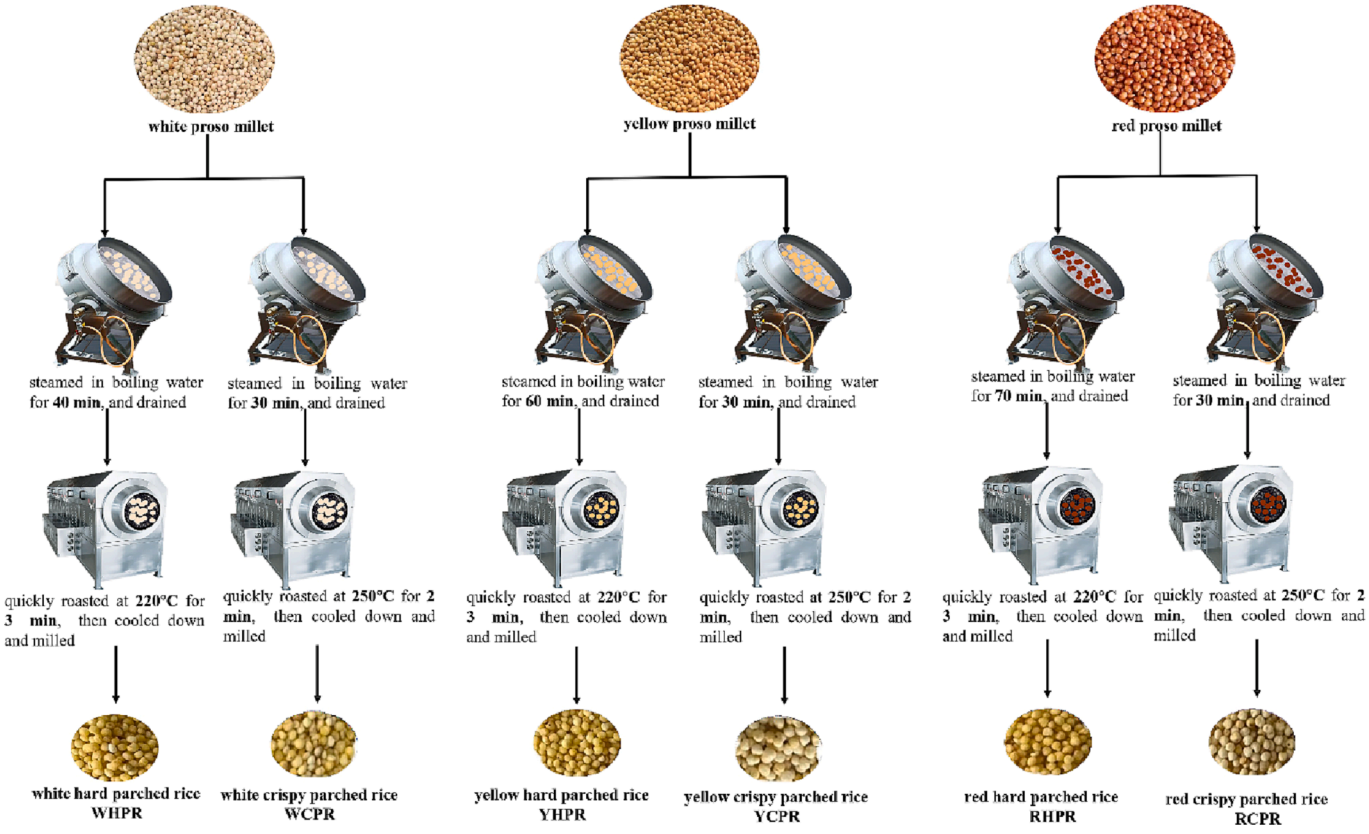


**Fig. 1.** The preparation flow chart of parched rice.

#### 2.4.3. Fourier transfer infrared spectrometry

Fourier transfer infrared spectrometry (FTIR) was conducted on an FTIR instrument (VETEX70, Bruker, German). Referring to the previous study with some modifications (Kumar et al., 2020), the sample was mixed with dried KBr at 1:100 m/m and subjected to a vacuum compression for pressing into slices. The operation was performed within the scanning wavelength range of 400–4000 $cm^{-1}$.

### 2.5. Thermal analysis

Thermal analysis was conducted using differential scanning calorimetry (DSC Q200, Waters, USA). Initially, 2.0 mg of sample was loaded into an aluminum crucible and mixed with distilled water at 1:3 ratio. Measurements were conducted in $N_2$ environment at 40 mL/min flow rate. The scanning temperature ranged within 30–300 °C /min with an increased rate of 10 °C /min (Ma et al., 2020).

### 2.6. Pasting properties

The pasting properties of samples were analyzed according to the method by Lu, Xu, Zhan, Chen, Jin, and Tian (2020) by using a rapid viscosity analyzer (RVA) (Newport Scientific, NSW, Australia). The sample (2.5 g) and 25 mL of distilled water were thoroughly mixed and heated at 50 °C for 1 min, slowly raised to 95 °C, held for 2.5 min, and then maintained at that temperature for 2 min. During pasting, the samples were homogenized at 960 rpm in the first 10 s and thereafter at 169 rpm for the rest of the test.

### 2.7. Rheological measurements

According to Jiang, Du, Zhao, Jiang, Yu, and Du (2020), the sample was pretreated with a rapid viscosity analyzer (RVA, Newport Scientific, NSW, Australia) to make a homogeneous paste. Rheological measurements were performed on a rheometer (DHR-1, Waters, USA) with a 40 mm parallel plate and a 0.1 mm gap. For stable shearing determination, the shear rate ranged within 0.1–1000 $s^{-1}$, and the changes in shear stress ($\tau$) and apparent viscosity ($\eta$) were recorded. The dynamic rheological measurement was performed at 25 °C with a frequency sweep of 10 rad/s in the linear viscoelastic region of 0.5% strain. Shear rate ranged within 0.01–100 Hz, and the storage modulus (G') and loss modulus (G'') were recorded.

### 2.8. In vitro digestibility

Referring to the study by Gao et al. (2022) with slight modifications, a 1.0 g of sample was placed in a tube, mixed with 5.0 mL of pepsin solution (2500 U/mL), and shaken in a water bath at 37 °C for 30 min. After the treatment, 50 mL of NaOH solution (0.01 mol/L), 20 mL of phosphate buffer solution (pH 6.8, 0.1 mol/L), and 5.0 mL of mixed amylase solution (1000 U/mL α-amylase and 3000 U/mL glucosidase) were added. Subsequently, the mixture was cultivated in a shaking water bath at 37 °C for 2 h. The solution (1 mL) was collected and mixed with 4 mL of ethanol to inactivate the enzymes after incubating for 0, 20, and 120 min. The solution was then centrifuged at 3800 r/min to collect the supernatant, and glucose content was measured by the dinitrosalicylic acid method. The content of rapidly digestible starch (RDS), slowly digestible starch (SDS), and resistant starch (RS) in the sample were calculated as follows:

$$\mathrm{RDS}(\%) = \frac{(G_{20} - G_0) \times 0.9}{TS} \times 100$$

$$\mathrm{SDS}(\%) = \frac{(G_{120} - G_{20}) \times 0.9}{TS} \times 100$$

$$\mathrm{RS}(\%) = \text{1-RDS-SDS}$$

where $G_0$, $G_{20}$, and $G_{120}$ are the glucose content of the solution after 0, 20, and 120 min of cultivation.

### 2.9. Flavor analysis

#### 2.9.1. HS-SPME/GC–MS analysis

The volatile compounds of samples were extracted by HS-SPME according to a previous study (Cai et al., 2020). The sample (5.0 g) was placed in the headspace vials, and a DVB/CAR-PDMS solid-phase extraction fiber (Supeloco, USA) was inserted to adsorb volatile compounds at 65 °C for 35 min. The analyses were performed on GC–MS (GCMS-QP2010 Ultra, Shimadzu, Japan). Volatile compounds were separated on a PEG-200 capillary column with helium carrier gas at a 0.8 mL/min flow rate. The custom temperature program was performed as follows: the column temperature was held at 40 °C for 30 min, ramped at 4 °C/min to 120 °C, then ramped at 4 °C/min to 120 °C followed by an increase of 6 °C/min to 240 °C and held for 12 min. The MS conditions were as follows: the interface temperature and ion source temperature were 250 °C and 200 °C, respectively; the ionization energy was 70 eV, and detection was performed at a voltage of 350 V and an emission current of 200 μA.

#### 2.9.2. E-nose analysis

E-nose analyses were conducted using a PEN3 e-nose (Airsense, Germany), which comprised sensor-array units, an automatic sampler, and pattern-recognition software. The sensor array comprised 10 metal-oxide semiconductors (W1C, W5S, W3C, W6S, W5C, W1S, W1W, W2S, W2W, and W3S). Each type of sensor element corresponded with different sensitive substances, including aromatic, broadrange, aromatic, hydrogen, arom-aliph, broad-methane, sulfur-organic, broad-alcohol, sulf-chlor, and methanealiph, respectively. The sample (5.0 g) was placed in a 40 mL of sample bottle and incubated at room temperature for 240 min. The sample was collected for 60 s, the sensor cleaning time was 300 s, and the injection flow rate was 400 mL/min for 5 s. Samples from 52 to 56 s were selected as representatives for analysis.

### 2.10. Statistical analysis

All trials were performed in triplicate. Data were analyzed by one-way fixed-effects analysis of variance (ANOVA) test using statistical software (SPSS 18.0, SPSS Inc., Chicago, IL, USA).

## 3. Results and discussion

### 3.1. Proximate composition

The proximate compositions of samples are listed in Table 1. The total starch, protein, and lipid contents of parched rice (74.20%,10.50%, and 2.19% for hard parched rice, and 70.98%, 10.00%, and 1.98% for crispy parched rice) were lower than that of raw proso millet (78.50%, 15.40%, and 2.53%). These results may be due to starch gelatinization, protein denaturation, lipid degradation, and the formation of starch–-protein/lipid complexes during thermal treatment (Wani, Hamid, Hamdani, Gani, & Ashwar, 2017). The ash content of samples also differed, with a higher content of raw proso millet (0.76%), followed by crispy parched rice (0.75%), and the lowest content of hard parched rice (0.46%). The steaming treatment may have caused the difference in ash content, where the hard parched rice was treated for a longer time and the soluble mineral was dissolved fully and endowed with the lowest ash content (Kumar et al., 2020). The amylose content of raw proso millet and parched rice also exhibited differences. Amylose content was the highest in raw proso millet (18.73%–20.42%), followed by hard parched rice (16.11%–16.78%) and the lowest in crispy parched rice (13.55%–14.29%). During the thermal treatment, starch in the samples was degraded, and the hydrogen bonds and glycosidic linkages were broken, leading to amylose leaching (Yang et al., 2018; Lu et al., 2020). Owing to

**Table 1**
Proximate compositions and *in vitro* digestibility properties of samples.

| Sample | | Moisture (%) | Total starch (%) | Protein (%) | Lipid (%) | Ash (%) | Amylose content (%) | RDS (%) | SDS (%) | RS (%) |
|---|---|---|---|---|---|---|---|---|---|---|
| Raw proso millet | WPR | 11.64 ± 0.04$^{a}$ | 73.20 ± 0.78$^{cd}$ | 15.73 ± 0.11$^{b}$ | 2.60 ± 0.13$^{a}$ | 0.86 ± 0.03$^{b}$ | 18.73 ± 0.05$^{c}$ | 19.67 ± 0.23$^{g}$ | 9.60 ± 0.23$^{j}$ | 70.73 ± 0.10$^{c}$ |
| | YPR | 11.26 ± 0.04$^{a}$ | 82.07 ± 0.77$^{a}$ | 14.31 ± 0.06$^{c}$ | 2.57 ± 0.16$^{a}$ | 0.68 ± 0.02$^{c}$ | 20.19 ± 0.05$^{b}$ | 10.66 ± 0.21$^{h}$ | 12.60 ± 0.30$^{f}$ | 76.75 ± 0.17$^{a}$ |
| | RPR | 11.51 ± 0.05$^{a}$ | 80.24 ± 0.50$^{ab}$ | 16.16 ± 0.04$^{a}$ | 2.42 ± 0.12$^{ab}$ | 0.74 ± 0.02$^{c}$ | 20.42 ± 0.05$^{a}$ | 11.80 ± 0.10$^{i}$ | 12.84 ± 0.19$^{f}$ | 75.36 ± 0.30$^{b}$ |
| | Mean | 11.47 ± 0.18A | 78.50 ± 4.22A | 15.40 ± 0.86A | 2.53 ± 0.14A | 0.76 ± 0.09A | 19.78 ± 0.82A | 14.04 ± 4.39C | 11.68 ± 1.62C | 74.28 ± 2.82A |
| Hard parched rice | WHPM | 3.78 ± 0.32$^{c}$ | 70.78 ± 0.12$^{de}$ | 10.02 ± 0.16$^{e}$ | 2.55 ± 0.00$^{a}$ | 0.49 ± 0.02$^{d}$ | 16.27 ± 0.11$^{e}$ | 57.76 ± 0.20$^{d}$ | 30.73 ± 0.11$^{b}$ | 11.52 ± 0.11$^{h}$ |
| | YHPM | 3.54 ± 0.29$^{c}$ | 76.23 ± 0.59$^{bc}$ | 10.15 ± 0.02$^{e}$ | 2.07 ± 0.05$^{cd}$ | 0.46 ± 0.03$^{d}$ | 16.11 ± 0.01$^{e}$ | 46.34 ± 0.09$^{f}$ | 31.82 ± 0.01$^{a}$ | 21.85 ± 0.09$^{d}$ |
| | RHPM | 3.40 ± 0.35$^{c}$ | 75.61 ± 2.04$^{c}$ | 11.33 ± 0.21$^{d}$ | 1.96 ± 0.03$^{d}$ | 0.44 ± 0.04$^{de}$ | 16.78 ± 0.05$^{d}$ | 55.56 ± 0.09$^{e}$ | 29.42 ± 0.03$^{c}$ | 15.03 ± 0.09$^{e}$ |
| | Mean | 3.57 ± 0.30B | 74.20 ± 2.83AB | 10.50 ± 0.66B | 2.19 ± 0.28B | 0.46 ± 0.03B | 16.39 ± 0.32B | 53.22 ± 5.42B | 30.66 ± 1.08A | 16.13 ± 4.70B |
| Cripsy parched rice | WCPR | 3.58 ± 0.11$^{c}$ | 70.99 ± 2.16$^{de}$ | 9.06 ± 0.39$^{g}$ | 2.22 ± 0.04$^{bc}$ | 0.39 ± 0.04$^{e}$ | 13.55 ± 0.01$^{h}$ | 62.46 ± 0.32$^{a}$ | 28.75 ± 0.43$^{c}$ | 8.80 ± 0.14$^{i}$ |
| | YCPR | 3.21 ± 0.13$^{c}$ | 67.73 ± 2.92$^{e}$ | 9.49 ± 0.05$^{f}$ | 1.86 ± 0.14$^{d}$ | 0.89 ± 0.01$^{b}$ | 14.29 ± 0.05$^{f}$ | 61.29 ± 0.11$^{b}$ | 26.16 ± 0.11$^{e}$ | 12.56 ± 0.05$^{g}$ |
| | RCPR | 4.73 ± 0.25$^{c}$ | 74.24 ± 3.27$^{cd}$ | 11.47 ± 0.09$^{d}$ | 1.86 ± 0.02$^{d}$ | 0.97 ± 0.04$^{a}$ | 13.87 ± 0.11$^{g}$ | 59.03 ± 0.29$^{c}$ | 27.17 ± 0.29$^{d}$ | 13.81 ± 0.03$^{f}$ |
| | Mean | 3.84 ± 0.72B | 70.98 ± 3.64B | 10.00 ± 1.16B | 1.98 ± 0.20B | 0.75 ± 0.28A | 13.90 ± 0.34C | 60.92 ± 1.57A | 27.36 ± 1.19B | 11.72 ± 2.34C |

Data are mean ± standard deviations ($n = 3$), and the values followed by different letters in the same column indicate the significant difference ($P < 0.05$).

the high temperature, the compact structure of amylose may have been disrupted during steaming, thereby enhancing the interaction between amylose and protein/lipid during roasting, and changing the amylose content (Yang, Hao, Wu, Liu, & Ouyang, 2021).

### 3.2. Structure characterization

#### 3.2.1. Morphology property

As demonstrated in Fig. 2, the starch granules in raw proso millet

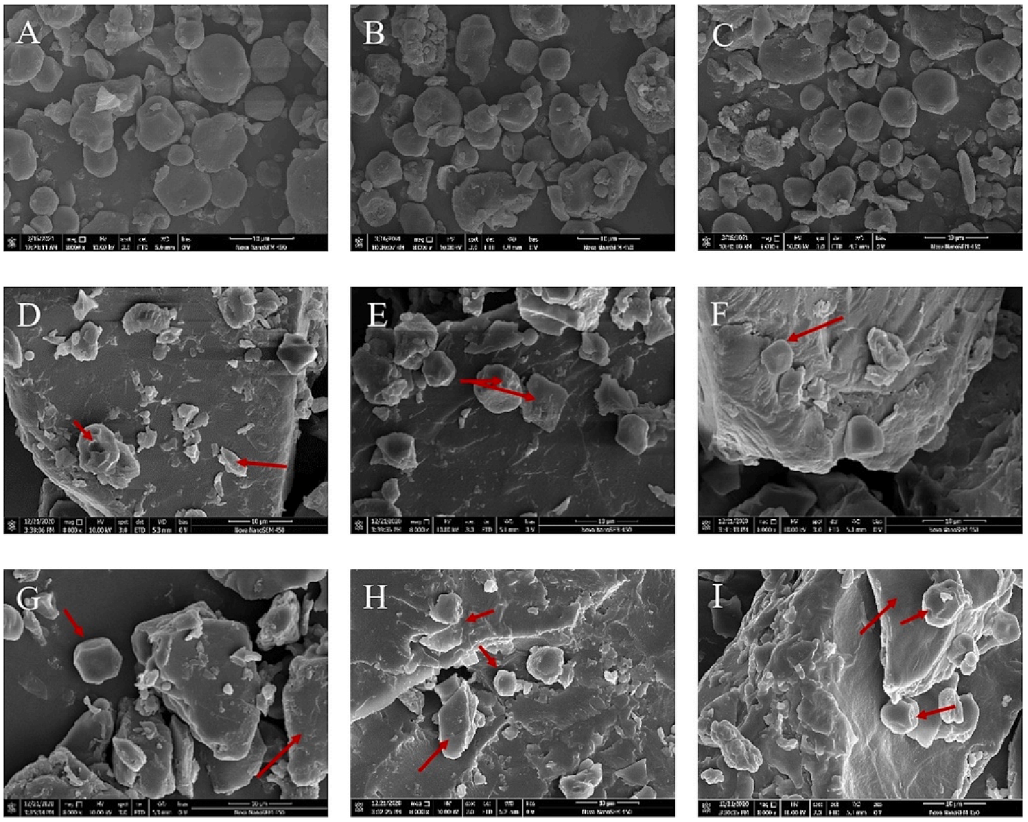


**Fig. 2.** Scanning electron microscope images of samples. (A) white proso millet, (B) yellow proso millet, (C) red proso millet, (D) white hard parched rice, (E) yellow hard parched rice, (F) red hard parched rice, (G) white crisp parched rice, (H) yellow crisp parched rice, (I) red crisp parched rice. (For interpretation of the references to colour in this figure legend, the reader is referred to the web version of this article.)

were primarily spherical or oval and covered with an uneven protein coating all around. The structure of parched rice starch was damaged, and the starch granules had an irregular shape with a rough surface. Hard and crispy parched rice showed more chunky and flaky protein films, and small partials can be observed surrounding it. The starch pasting and cleavage, protein denaturation, fiber splitting, and starch granules absorbing water and expanding until rupture caused by steaming and roasting treatment can be the causes of the considerable changes in morphology of parched rice (Zhao, Jiao, Yang, Liu, & Jin, 2021). The starch molecules also adhered onto one another through pasting and formed many adhesive granules. The steaming and roasting procedures may have likely induced such changes in morphology because thermal treatment always promoted granule swelling, gelatinization, and shape modification. Meanwhile, the soluble substances (such as polysaccharides, protein, and amylose) may have been dissolved, causing the granules to aggregate and adhere (Yang et al., 2018). The center of the parched rice starch granules contained depressions of various sizes, which may be related to the damage during thermal treatment, where the linkages in samples were broken down, and the structure was disrupted (Ding, Yang, Xia, Wu, Zhou, & Wang, 2018).

### 3.2.2. Crystalline property

The helical structure formed by amylose was confirmed to constitute a crystalline region in starch, and the amylose dispersed between amylopectin constituted the amorphous region of starch. According to crystal structures, natural starches can be divided into A, B, and C types. Among them, the A-type crystal structure was the most compact, and it was the crystal structure of most cereal starch (Wang, Zhong, Zheng, Zhang, & Zeng, 2023). When starch formed complexes with fatty acids or alcohols, it may form a V-type crystal structure (Jiang et al., 2022). All raw proso millets displayed typical A-type crystal structures with strong diffraction peaks at 15°, 17°, 18°, and 23° (Fig. 3A). The crystal types changed to V-type after thermal treatment, and new diffraction peaks appeared at 13° and 20° for hard parched rice, and 20° for crispy parched rice. The thermal treatment changed the crystal type probably because the starch crystal structure was disrupted and the double-helix structure was lost. The starch–lipid complex formed in parched rice may also cause the transformation of crystal type (Olamiti, Takalani, Beswa, & Jideani, 2020). The change in crystal type of hard parched rice and crispy parched rice was similar to that in the study of Dharmaraj, Parameswara, Somashekar, and Malleshi (2014), in which the crystalline structure of corn changed during hydrothermal treatment, peeling, swelling, and bursting. These results indicated that thermal and physical processing treatment can effectively change the crystallization type of grains. According to Table 2, the crystallinity of raw proso millet was 29.81%–37.35%, whereas the crystallinity of the corresponding parched rice was lower (with 21.65%–23.58% for hard parched rice and 25.64%–28.05% for crispy parched rice). The thermal treatment reduced the crystallinity of parched rice, indicating that the treatment destroyed the crystalline regions and internal structure of the starch. The crystallite disruption due to the starch gelatinization and reorientation of the double helix forming the crystal column primarily led to a decrease in sample crystallinity (Olamiti et al., 2020).

### 3.2.3. FTIR analysis

All samples exhibited similar FTIR spectra, which are depicted in Fig. 3B. The peaks ranging within the absorption bands at 3500–3400 $cm^{-1}$ were attributed to the stretching of the —OH bond. The leftward shift of the —OH absorption peak in parched rice demonstrated that the thermal treatment decreased the hydrogen bond content and increased the content of disordered molecules in the sample (Sun, Gong, Li, & Xiong, 2014). Compared with raw proso millet, parched rice showed a more significant absorption peak at 2926 $cm^{-1}$, suggesting that thermal treatment allowed for effective interaction of —OH with other molecules. The stretching of —C═O caused the absorption peaks in 1690–1630 $cm^{-1}$, and the amide appeared in 1690–1650 $cm^{-1}$. The raw proso millet exhibited a more vigorous peak intensity of amide groups, suggesting a higher protein content (Long, Ji, Pan, Sun, Li, & Qin, 2015). The absorption peaks at 1340–1020 $cm^{-1}$ indicated the presence of —C═O or —C≡N stretching vibrations in parched rice, and the peak appearing at 1078 $cm^{-1}$ was caused by the skeletal vibrations of α-1,4 glycosidic bonds. The absorption peaks at 1000–1250 $cm^{-1}$ were observed in parched rice, suggesting that the starch in parched rice interacted with the non-starch components (Sun et al., 2014). FTIR can characterize special functional groups and provide relevant information about the structural properties of starch. The absorption peak around 1045 $cm^{-1}$ was correlated with the crystalline region of starch, that at 1022 $cm^{-1}$ was related to the amorphous region of starch, that at 995 $cm^{-1}$ was caused by the ordered structure of hydrogen bonds formed between starch molecules (Du, Jiang, Jiang, Ge, & Du, 2020). Therefore, ratios of 1047/1022 $cm^{-1}$ ($R_{1047/1022}$) and 995/1022 $cm^{-1}$ ($R_{995/1022}$) were commonly used as indices to evaluate the degree of order within starch. The $R_{1047/1022}$ reflected the degree of order, whereas $R_{995/1022}$ indicated the level of the double helix (Gao et al., 2022). The $R_{1047/1022}$ and $R_{995/1022}$ of parched rice samples were lower than those of raw proso millet (Table 2), indicating that the crystal structure of starch in parched rice was more disordered, consistent with the results of crystalline properties. Thermal treatment always disrupted the native structure of starch, cleaved the whole granules, and reduced the crystallinity of samples (Ding et al., 2018). As a result, parched rice was endowed with depression on its surface and broken into fragments (Fig. 2).

### 3.2.4. Second structure of the protein

The amide I and III bands of the protein in the FTIR spectra can be used to characterize its secondary structure. The amide III bands were represented by the α-helix (1295–1330 $cm^{-1}$), β-sheet (1220–1250 $cm^{-1}$), β-turn (1270–1295 $cm^{-1}$), and irregular curl (1250–1270 $cm^{-1}$) (Long et al., 2015). The content of each structure was calculated by deconvolution and shown in Table 2. Compared with raw proso millet, the β-sheet content of crispy parched rice and hard parched rice was reduced, whereas the β-turn and α-helix contents increased. These results indicated that the secondary structure of parched rice protein changed significantly after thermal treatment possibly due to the conversion of β-sheet to α-helix and β-turn. After thermal treatment, the subunit proteins in samples expanded, and the hydrophobic groups were exposed to the polar environment to form protein aggregates (Gulati, Li, Holding, Santra, Zhang, & Rose, 2017). The β-sheet was located inside the protein, and protein aggregation decreased its fraction (Long et al., 2015). The conversion of the β-sheet to the α-helix was similar to the results of Gulati, Li, Holding, Santra, Zhang, and Rose (2017) for thermal treatment of millet. This finding indicated that thermal treatment can effectively disrupt the intermolecular hydrogen bonding and promote the formation of protein hydrophobic groups and the conversion of secondary structure in cereals.

## 3.3. Thermal properties

The thermal properties of different samples are shown in Table 3. The $T_O$ of raw proso millet was observed at around 65.88–68.13 °C, which was associated with the starch crystalline melting and gelatinization. The $T_O$ of parched rice was observed at around 102.73–120.12 °C, which was related to the melting of amylose–lipid complexes. Additionally, the $T_P$ and $T_C$ of parched rice were higher than those of raw proso millet, indicating that thermal treatment endowed different thermal properties to parched rice. The significant increase in $T_O$ may be attributed to the transformation of the crystalline region to an amorphous inner structure of starch granules (Kumar et al., 2020), which meant that the parched rice required higher temperature to destroy the crystallinity and helix order in samples. During thermal treatment, pregelatinization, crystalline structure disintegration, and chain degradation affected the structure of parched rice, leading to

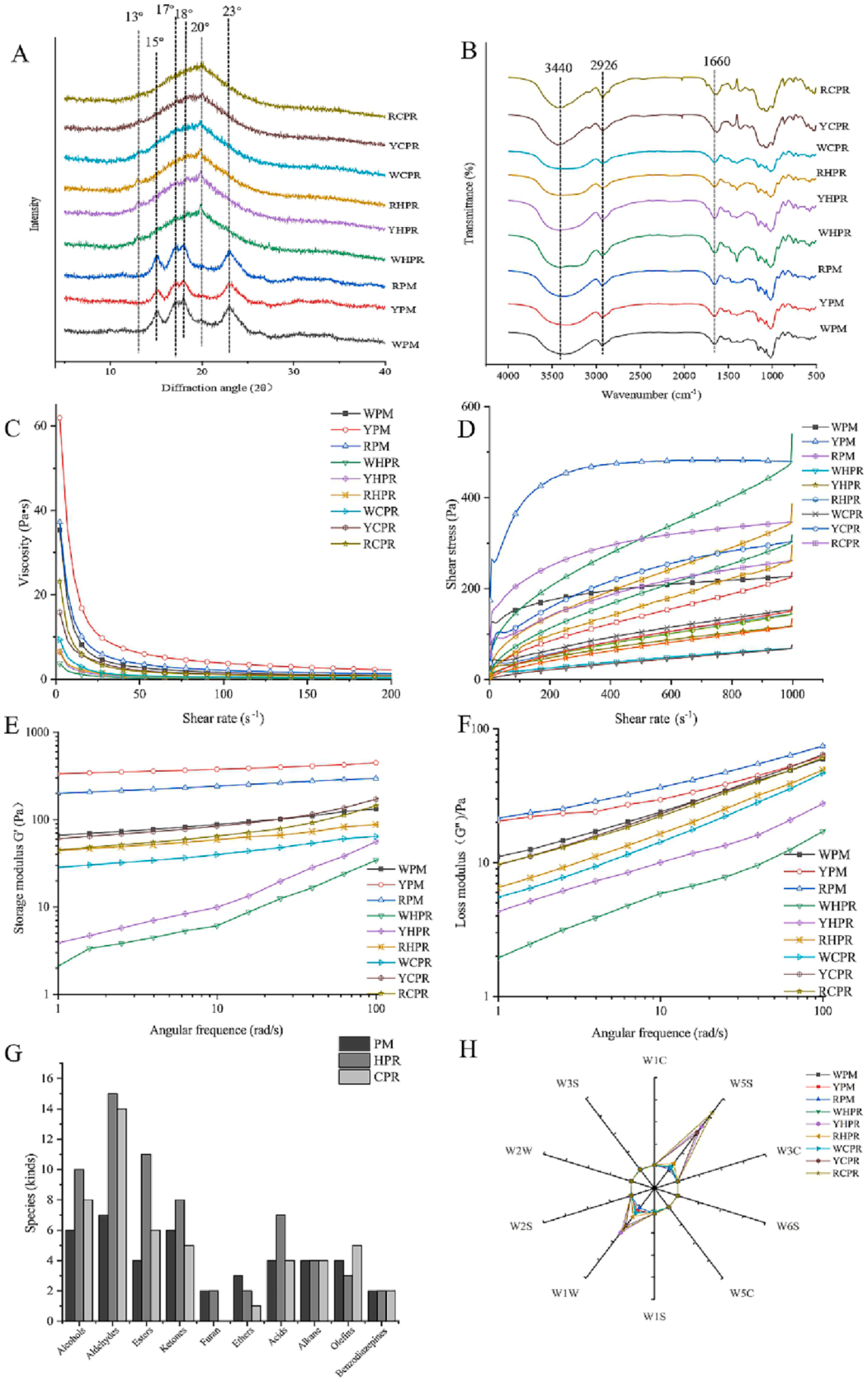


**Fig. 3.** (A) The XRD spectra of samples. (B) The FTIR spectra of samples. (C) The shear thinning of sample pastes. (D) The rheopexy properties of sample pastes. (E) and (F) The frequency scanning curves of sample pastes. (G) Comparison of volatile species in different varieties of samples. (H) The E-nose analysis of samples.

**Table 2**
Structural parameters of samples and Secondary structure of protein in samples.

| Sample | | Crystallinity % | Crystal type | $R_{1047/1022}$ | $R_{995/1022}$ | β-sheet | random coil | α-helix | β-turn |
|---|---|---|---|---|---|---|---|---|---|
| Raw proso millet | WPM | 35.89 ± 0.51$^{b}$ | A | 1.065 ± 0.001$^{b}$ | 1.074 ± 0.004$^{b}$ | 49.49 ± 0.82$^{a}$ | 7.92 ± 0.12$^{c}$ | 8.24 ± 0.33$^{gh}$ | 34.36 ± 0.37$^{f}$ |
| | YPM | 37.35 ± 1.56$^{a}$ | A | 1.082 ± 0.003$^{a}$ | 1.066 ± 0.007$^{b}$ | 48.30 ± 0.57$^{a}$ | 7.61 ± 0.20$^{c}$ | 8.57 ± 0.059 $^{fg}$ | 35.52 ± 0.43$^{e}$ |
| | RPM | 29.81 ± 0.46$^{c}$ | A | 1.086 ± 0.001$^{a}$ | 1.094 ± 0.001$^{a}$ | 46.49 ± 0.41$^{b}$ | 8.09 ± 0.05$^{c}$ | 7.58 ± 0.08 $^{h}$ | 37.84 ± 0.45$^{b}$ |
| | Mean | 34.35 ± 4.00A | | 1.078 ± 0.001A | 1.094 ± 0.014A | 48.09 ± 1.44A | 7.87 ± 0.24B | 8.13 ± 0.48B | 35.90 ± 1.62B |
| Hard parched rice | WHPR | 21.65 ± 0.18$^{f}$ | V | 0.901 ± 0.003$^{d}$ | 0.944 ± 0.001$^{d}$ | 41.64 ± 0.81$^{d}$ | 7.60 ± 0.030$^{c}$ | 13.39 ± 0.66 $^{cd}$ | 37.38 ± 0.19$^{bcd}$ |
| | YHPR | 23.01 ± 0.71$^{de}$ | V | 0.900 ± 0.001$^{d}$ | 0.950 ± 0.000$^{d}$ | 42.61 ± 0.74$^{d}$ | 6.99 ± 0.028$^{d}$ | 13.75 ± 0.30$^{c}$ | 36.65 ± 0.47$^{d}$ |
| | RHPR | 23.58 ± 0.78$^{de}$ | V | 0.998 ± 0.007$^{c}$ | 0.989 ± 0.010$^{c}$ | 39.85 ± 0.21$^{e}$ | 7.72 ± 0.01$^{c}$ | 15.54 ± 0.44$^{a}$ | 36.89 ± 0.21$^{bcd}$ |
| | Mean | 22.75 ± 0.99B | | 0.933 ± 0.056B | 0.961 ± 0.024B | 41.37 ± 1.35B | 7.44 ± 0.35C | 14.22 ± 1.10A | 36.97 ± 0.41AB |
| Crispy parched rice | WCPR | 28.05 ± 0.77$^{c}$ | V | 0.903 ± 0.004$^{d}$ | 0.942 ± 0.001$^{d}$ | 38.73 ± 0.76e | 9.98 ± 0.00$^{a}$ | 14.56 ± 0.52$^{b}$ | 36.73 ± 0.24 $^{cd}$ |
| | YCPR | 25.64 ± 0.96$^{d}$ | V | 0.904 ± 0.003$^{d}$ | 0.950 ± 0.001$^{d}$ | 35.41 ± 0.01e | 10.28 ± 0.29$^{a}$ | 13.14 ± 0.34 $^{cd}$ | 41.17 ± 0.06$^{a}$ |
| | RCPR | 25.90 ± 0.57$^{d}$ | V | 0.991 ± 0.005$^{c}$ | 0.994 ± 0.004$^{c}$ | 39.12 ± 0.57$^{f}$ | 10.43 ± 0.61$^{a}$ | 12.78 ± 0.35$^{d}$ | 37.67 ± 0.38$^{bc}$ |
| | Mean | 26.53 ± 8.15B | | 0.933 ± 0.295B | 0.962 ± 0.313B | 37.75 ± 1.87C | 10.23 ± 0.36A | 13.49 ± 0.90A | 38.52 ± 2.10A |

Data are mean ± standard deviations ($n = 3$), and the values followed by different letters in the same column indicate the significant difference ($P < 0.05$).

changes in thermal properties (Ma et al., 2020). According to the XRD results, the crystal type of raw proso millet changed from A-type to V-type due to the thermal treatment, indicating the formation of amylose–lipid, leading to changes in the thermal properties of parched rice (Olamiti et al., 2020). A narrower gelatinization temperature range ($T_C$-$T_O$) was observed for parched rice (with a mean value of 14.91 °C for raw proso millet, 5.63 °C for hard parched rice, and 4.8 °C for crispy parched rice). These results may be attributed to the fact that thermal treatment promoted the fusion of low cohesion crystals, reduced the energy required for melting, and enhanced the interaction between the remaining crystal chains (Duque, Leong, Agyei, Singh, Larsen, & Oey, 2020). The gelatinization enthalpy ($\Delta H$) of starch was related to its crystal structure and crystallinity. A higher $\Delta H$ demonstrated a more ordered crystalline structure, a higher double-helix content, and greater thermal stability of starch (Du et al., 2020). The $\Delta H$ of parched rice (with 0.145–0.253 J/g of hard parched rice and 0.226–0.463 J/g of crispy parched rice) was lower than that of raw proso millet (10.770–11.060 J/g), suggesting that less energy was needed to melt the crystalline structure and amylose double helix in parched rice (Duque et al., 2020). This result may be attributed to the previous disruption of the highly ordered structure in parched rice during thermal treatment, leading to a more flexible structure, degraded crystalline area, and decreased crystallinity (Table 2). The hard parched rice was steamed and roasted for a longer period, inflicting greater structural damage and conferring the lowest $\Delta H$.

### 3.4. Pasting properties

The pasting properties of raw proso millet and parched rice are summarized in Table 3, including peak viscosity (PV), breakdown viscosity (BV), final viscosity (FV), setback viscosity (SV), and pasting temperature (PT). The pasting property parameters of parched rice were lower than those of raw proso millet, indicating that a lower viscosity was endowed to parched rice during pasting. The lower BV of parched rice revealed that the molecular chains in parched rice were disrupted, and the force between amylose and the branched chains was diminished (Du et al., 2020). The decreasing tendency of SV observed in parched rice indicated that steaming and roasting procedures induced the amylose retrogradation level and inhibited the formation of double-helix structure for the reassociation and recrystallization of amylopectin external glucan chains (Duque et al., 2020). The retrogradation ability reduction of parched rice may have positive significance for processing proso millet products, because retrogradation usually leads to a decrease in quality, such as increased dehydration and hardness. The lower PV and FV observed for parched rice demonstrated that steaming and roasting may disrupt the highly ordered structure in parched rice (Ma et al., 2020). The reduction in viscosity after thermal treatment may also be due to the pregelatinization, which caused the water absorption and swelling of starch granules, as well as the looser rearrangement of starch chains. The swelling ability was reduced when the sample was heated again, making it easier to disintegrate into pieces and reduce the viscosity (Duque et al., 2020). The thermal treatment also affected the PT of samples by improving the PT value of crispy parched rice to 92.53 °C and it cannot even be detected for hard parched rice. This result may be caused by the higher degree of pregelatinization and damage to the starch structure due to the thermal treatment. In addition to starch, other components in proso millet (such as soluble dietary fiber) may also play an essential role in its viscosity profile. In this study, hard parched rice was steamed in boiling water for a longer time, and the soluble substances were dissolved to a greater extent, thereby exhibiting the lowest viscosity. During the thermal treatment, starch may also interact and reassociate with protein or lipid to form complexes similar to chemical cross-linking modified starch, thereby restricting the swelling and gelatinization of samples (Lu et al., 2020).

### 3.5. Rheological properties

#### 3.5.1. Rheology character

The shear stress and shear rate of samples were analyzed by the Herschel–Bulkley equation ($\tau = \tau_0 + K\gamma^n$). The results of the rheology characterization are shown in Table 3. The flow properties can be well described by the model with high regression coefficients ($R^2 > 0.98$). The characteristic flow index ($n$) was<1 for all samples, indicating that the paste structures were easy to shear, had pseudoplastic characteristics, and belonged to non-Newtonian fluids (Jiang et al., 2020). The stress force ($\tau_0$, the finite stress required of the sample to achieve flow state) of raw proso millet was too high to be detected, whereas the $\tau_0$ of hard parched rice ranged from 12.28 Pa to 22.93 Pa, and the $\tau_0$ of crispy parched rice ranged from 29.1 Pa to 50.36 Pa. The viscosity coefficient ($K$) of raw proso millet paste (46.28–218.47 Pa·s$^n$) was higher than that of parched rice (with hard parched rice of 0.13–0.57 Pa·s$^n$, and crispy parched rice of 0.67–10.61 Pa·s$^n$). Compared with raw proso millet, the $\tau_0$ and $K$ of parched rice decreased, indicating that the paste formed by parched rice required higher stress to achieve the same deformation as the raw proso millet. In other words, parched rice paste showed greater shear stability and higher shear-thinning behavior, indicating that thermal treatment limited the exudation and swelling of starch in parched rice (Lu et al., 2020).

#### 3.5.2. Shear-thinning behavior

Shear-thinning behavior, an evident inherent characteristic of a pseudoplastic fluid, is the phenomenon where the apparent viscosity of

**Table 3**
The thermal parameters from DSC thermograms, Herschel-Bulkley parameters and pasting properties of samples.

| Sample | $T_O$ (°C) | $T_P$ (°C) | $T_C$ (°C) | $T_C$-$T_O$ (°C) | $\Delta H$ (J/g) | $\tau_0$/Pa | $K$/ Pa·$s^n$ | $n$ | $R^2$ | Ring area/ Pa·$s^{-1}$ | PV/cP | BV/cP | FV/cP | SV/cP | PT/°C |
|---|---|---|---|---|---|---|---|---|---|---|---|---|---|---|---|
| WPM | 68.13 ± 0.69$^{d}$ | 74.13 ± 0.36$^{d}$ | 81.40 ± 0.60$^{d}$ | 12.36 | 10.770 ± 0.57$^{a}$ | — | 46.28 | 0.2034 | 0.9947 | 59647$^{e}$ | 1465.33 ± 2.08$^{b}$ | 598.33 ± 3.79$^{b}$ | 3736.67 ± 15.50$^{b}$ | 2867.33 ± 25.81$^{b}$ | 88.12 ± 0.08$^{bc}$ |
| YPM | 65.88 ± 0.09$^{d}$ | 73.94 ± 0.16$^{d}$ | 82.91 ± 0.34$^{d}$ | 17.21 | 11.060 ± 0.31$^{a}$ | — | 218.47 | 0.1222 | 0.9993 | 151263$^{a}$ | 2051.00 ± 6.56$^{a}$ | 928.33 ± 21.78$^{a}$ | 4136.67 ± 65.07$^{a}$ | 3019.33 ± 46.70$^{a}$ | 85.65 ± 0.11$^{cd}$ |
| RPM | 66.49 ± 0.77$^{d}$ | 74.68 ± 0.04$^{d}$ | 81.21 ± 0.17$^{d}$ | 15.15 | 10.960 ± 0.04$^{a}$ | — | 84.01 | 0.2072 | 0.9935 | 77484$^{d}$ | 1098.67 ± 4.04$^{d}$ | 386.67 ± 1.53$^{c}$ | 2878.67 ± 32.35$^{c}$ | 2176.33 ± 27.59$^{c}$ | 89.15 ± 0.48$^{b}$ |
| Mean | 66.83 ± 1.14C | 74.25 ± 0.38C | 81.84 ± 0.89C | 14.91 | 10.930 ± 0.32A | — | 116.25 | 0.18 | — | 96131A | 1502.00 ± 408.70A | 602.10 ± 250.03A | 3395.40 ± 795.20A | 2499.30 ± 700.15A | 87.64 ± 1.58A |
| WHPR | 104.37 ± 0.52$^{c}$ | 106.83 ± 0.00$^{c}$ | 108.37 ± 0.52$^{c}$ | 4.73 | 0.145 ± 0.05$^{b}$ | 12.28 | 0.13 | 0.8854 | 0.9982 | 3458 $^{k}$ | 181.00 ± 8.89 g | 26.00 ± 1.73$^{f}$ | 289.33 ± 14.57 $^{g}$ | 134.33 ± 7.37 g | — |
| YHPR | 105.57 ± 1.03$^{c}$ | 109.53 ± 2.89$^{bc}$ | 110.56 ± 2.41$^{bc}$ | 7.42 | 0.168 ± 0.02$^{b}$ | 19.14 | 0.57 | 0.7459 | 0.9984 | 6188$^{i}$ | 152.50 ± 1.50 g | 19.00 ± 1.00$^{f}$ | 256.50 ± 3.50 g | 123.00 ± 1.00 g | — |
| RHPR | 104.79 ± 4.72$^{c}$ | 108.33 ± 4.21$^{c}$ | 111.40 ± 5.31$^{bc}$ | 4.73 | 0.253 ± 0.06$^{b}$ | 22.93 | 0.55 | 0.7818 | 0.9979 | 4355$^{j}$ | 193.00 ± 1.00 g | 27.50 ± 0.50$^{f}$ | 321.50 ± 1.50 g | 156.00 ± 1.00 g | — |
| Mean | 104.91 ± 2.24B | 108.23 ± 2.59B | 110.11 ± 2.97B | 5.63 | 0.189 ± 0.06B | 18.11 | 0.42 | 0.8 | — | 4667B | 175.50 ± 18.58C | 24.17 ± 4.06B | 289.11 ± 29.14C | 137.78 ± 15.00C | — |
| WCPR | 113.21 ± 1.71$^{b}$ | 115.07 ± 1.08$^{b}$ | 117.40 ± 1.11$^{ab}$ | 4.61 | 0.354 ± 0.01$^{b}$ | 29.1 | 0.67 | 0.7579 | 0.9976 | 9552 $^{h}$ | 501.50 ± 0.50$^{f}$ | 42.00 ± 3.00$^{f}$ | 841.00 ± 3.00$^{f}$ | 381.50 ± 0.50$^{f}$ | 92.53 ± 2.03$^{a}$ |
| YCPR | 120.12 ± 0.00$^{a}$ | 123.78 ± 0.00$^{a}$ | 124.06 ± 0.08$^{a}$ | 3.98 | 0.463 ± 0.00$^{b}$ | 34.39 | 10.61 | 0.4716 | 0.9937 | 38757$^{f}$ | 1175.00 ± 7.00$^{c}$ | 281.00 ± 2.00$^{d}$ | 1698.00 ± 10.00$^{d}$ | 804.00 ± 5.00$^{d}$ | 78.65 ± 0.40$^{e}$ |
| RCPR | 102.73 ± 0.94$^{c}$ | 105.05 ± 1.84$^{c}$ | 107.94 ± 1.80$^{c}$ | 5.82 | 0.336 ± 0.00$^{b}$ | 50.36 | 5.55 | 0.5307 | 0.9934 | 34624 $^{g}$ | 758.00 ± 59.00$^{e}$ | 101.50 ± 15.50$^{e}$ | 1236.50 ± 69.50$^{e}$ | 580.00 ± 26.00$^{e}$ | 83.98 ± 1.63$^{d}$ |
| Mean | 112.02 ± 7.88A | 114.63 ± 8.44A | 116.47 ± 7.31A | 4.8 | 0.385 ± 0.06B | 37.95 | 5.61 | 0.59 | — | 27644B | 501.50 ± 0.50B | 42.00 ± 3.00B | 841.00 ± 0.50B | 381.50 ± 0.50B | 92.53 ± 2.03A |

Data are mean ± standard deviations ($n$ = 3, and $n$ = 2 in DSC thermograms), and the values followed by different letters in the same column indicate the significant difference ($P < 0.05$).

the system decreases with increased shear rate under the effect of shear stress (Jiang et al., 2020). According to Fig. 3C, the apparent viscosity of the samples decreased and tended to be flat with increased shear rate, showing a shear-thinning behavior. This finding was also manifested as $n < 1$ in Table 3. The shear-thinning behavior of samples was due to the applied shear stress disrupting the molecular network in the paste. The sample pastes showed the following viscosity order within the experimental range: raw proso millet > crispy parched rice > hard parched rice. The lower viscosity of parched rice may be due to the pregelatinization of starch during the thermal treatment, where the starch chains rearranged, thereby inhibiting the expansion of starch molecules and preventing the formation of paste with higher viscosity (Qian et al., 2020). Moreover, the structural damage caused by thermal treatment to parched rice decreased its crystallinity (Table 2), making intermolecular forces weaker and hydrogen bonds more likely to be broken. Due to the longest steaming processing time, the hard parched rice exhibited the lowest viscosity and may undergo a greater degree of pregelatinization, thereby being endowed with the lowest viscosity.

### 3.5.3. *Thixotropy and restoring force of shear structure*

The thixotropic curves of different parched rice and raw proso millet are shown in Fig. 3D. The rheological curve experienced during the rise of shear stress from 0.1 $s^{-1}$ to 1000 $s^{-1}$ was the upward line, and the rheological curve experienced during the decline from 1000 $s^{-1}$ to 0.1 $s^{-1}$ was the downward line. The two curves were surrounded to form a hysteresis loop, and the loop area was correlated with and reflected the thixotropy of the sample. All samples exhibited clockwise hysteresis loops, indicating that the systems were significantly thixotropic. The thixotropy of different samples differed significantly, with raw proso millet having the higher hysteresis loop area (59647–151263 Pa·$s^{-1}$) and parched rice having the lower hysteresis loop area (with hard parched rice of 4355–6188 Pa·$s^{-1}$ and crispy parched rice of 9552–38757 Pa·$s^{-1}$) (Table 3). These findings may be related to the starch structure disruption and the formation of starch, lipid, and protein complexes. Starch gelatinization, particle expansion, and amylose molecular leaching occurred in the whole-grain system during the thermal treatment. The leached amylose from cereals and swollen starch granules can form complexes through the entanglement of molecular chains. The lipid and protein recombined with amylose or amylose by modifying their three-dimensional conformation, influencing the fluidity of samples (Lu et al., 2020). Among them, hard parched rice had the smallest ring area probably because the longest thermal treatment inflicted more structural damage and promoted the formation of more complex compounds (corresponding with the results in Table 2).

### 3.5.4. *Dynamic rheological properties*

Fig. 3E and Fig. 3F show the significant changes in the G' and G" of samples, indicating that thermal treatment can effectively affect the structure of parched rice paste. With increased scanning frequency, the G' and G" of parched rice paste became significantly greater than those of raw proso millet. The strong elasticity and gelation of the samples were caused by the lack of crossover between G' and G" within the scanning-frequency range. During scanning, the G' and G" of parched rice paste were lower than that of raw proso millet, and the G' and G" of hard parched rice paste were lower than that of crispy parched rice, indicating that the paste of parched rice was weaker than that of raw proso millet paste. This result may be due to the degradation of starch chains caused by thermal treatment, resulting in less entanglement and interaction of starch, thereby changing the network structure (Wani et al., 2017).

## 3.6. *In vitro digestibility*

According to Table 1, thermal treatment significantly increased the proportions of RDS and SDS in parched rice but reduced the RS content of parched rice. These changes may be the result of starch granules

breaking into smaller fragments (Fig. 2), which can enhance the interaction of starch with digestive enzymes and make it more conducive for human to digest and absorb (Vinutha et al., 2022). The pregelatinization during thermal treatment was conducted according to the RVA results, causing starch swelling, granule structure disruption, and crystallinity reduction. These may also lead to increased RDS and SDS content of parched rice. Generally, higher crystallinity and slower digestion are always associated with a more ordered structure of starch (Huong, Hoa, & Hung, 2021). During the thermal treatment, steaming and roasting procedures may have promoted the disruption of the double-helix structure within the starch granules, as evidenced by the results of reduced $\Delta H$ and short-range ordered crystallinity (Table 2 and Table 3). The crystalline region of starch was more resistant to enzymes, demonstrating that the amorphous region of starch was more likely to make contact with α-amylase than the crystalline region, and thus be degraded. Thermal treatment in this study may induce a certain degree of disruption to the crystal structure of parched rice, exposing its α-1,4 or α-1,6 glycosidic bonds that were originally hidden in the crystalline region. Consequently, RS content decreased and digestibility was improved (Solaesa, Villanueva, Vela, & Ronda, 2022). Notably, hard parched rice demonstrated more RS than crispy parched rice due to the longer roasting time and greater development of starch–lipid or starch–protein complexes. The lipid and protein usually interacted with amylose and formed starch-based complexes that restricted starch digestion (Duque et al., 2020). Although thermal treatment resulted in the formation of starch-based complexes in parched rice, the crystallinity of parched rice still decreased compared with that of raw proso millet (Table 2). These findings indicated that the formation of complexes exhibited a much lower impact on the sample structure than the disruption caused by seaming and roasting on the granules. Thus, although complex formation may lead to a slight increase in digestibility, severe structural damage resulted to a greater extent in more digestible parched rice. Overall, the increased RDS and SDS contents of parched rice demonstrated that thermal treatment effectively enhanced its *in vitro* digestibility. These findings confirmed that parched rice can be a potential food for rapidly elevating blood sugar levels to providing energy to the body.

### 3.7. Flavor analysis

#### 3.7.1. Identification of main flavor compounds

Flavor compounds are important components that provide food with a unique aroma, generally derived from amino acids, fatty acids, phenolic acids, and other nutrients. Due to the various reactions during thermal treatment, the raw grain materials and processed grains always exhibit completely different volatile characteristics. The evaporation of low-boiling compounds, the release of compounds present in the sample in a bound form, and the generation of additional compounds through chemical reactions all contributed to the formation of the distinctive aroma of thermal-treated grains (Lina & Min, 2022). The distribution of aroma flavor substances in raw proso millet and parched rice is displayed in Fig. 3G. Hard parched rice (HPR 63) was the most abundant in flavor substance species, higher than crispy parched rice (CPR 48) and raw proso millet (PM 42). Hard parched rice had the most alcohols and aldehydes (10 and 15), followed by esters and ketones (11 and 8), whereas crisp parched rice had fewer alcohols and aldehydes than hard parched rice (8 and 14). The differences suggested that a higher period of thermal treatment resulted in more flavor substances. Furthermore, the alcohols, aldehydes, and ketones in raw proso millet were the most diverse, with 6, 7, and 6 kinds. The detailed analysis of the types and quantities of volatile substances in raw proso millet and parched rice also revealed differences (Supplementary File). More flavor components were detected in parched rice (63 in hard parched rice and 48 in crispy parched rice) than in raw proso millet (42), suggesting that the thermal treatment gave parched rice a distinctive scent and richer flavor. As a result of thermal treatment, starch was degraded to small-molecule sugars, and the protein was denatured to small-molecule polypeptides. Additionally, the raw materials contained amino and reducing sugars. These substances underwent the Maillard reaction at a high temperature, resulting in a more intense flavor of parched rice (Heiniö et al., 2016).

Alcohols may be cause by carbohydrate metabolism, amino acid dehydrogenation, and decarboxylation in samples, and they always provided samples with fruit, nut, floral, sweet aromas, and other mellow aromas (Bi et al., 2021). Hard parched rice (10) and crispy parched rice (8) contained a wider variety of alcoholic substances than raw proso millet (6). Alcohols in parched rice primarily included ethanol, butanol, pentanol, hexanol, 1-octene-3-ol, and undecanol, which endowed the samples with wine, nut, and fruit aromas (Liu et al., 2012). Hard parched rice (15) and crispy parched rice (14) contained more aldehydes than raw proso millet (7). Aldehydes may be produced by the oxidation of fatty acids in grains and the Maillard reaction during thermal treatment (Zhang et al., 2020). Pentanal, hexanal, heptaldehyde, and nonanal were the most abundant aldehydes in raw proso millet, with hexanal having the highest content. Nonanal was equipped with a pleasant aroma that mellowed the overall aroma of parched rice (Liu et al., 2012). The hexanal content of parched rice was significantly higher than that in raw proso millet, which imparted greasy, grassy, and apple flavors to parched rice. (E, E)-2,4-Nonadienal and *trans*-2-decenal were detected in parched rice, possibly due to linolenic acid breakdown, and they contributed greasy and nutty aromas to the parched rice. Ethenyl ethanoate, hexalactone, and nonanolactone were exclusively found in parched rice among the esters. Compared with raw proso millet, the ethenyl ethanoate, pentyl formate, dimethyl glutarate, dimethyl adipate contents of parched rice were higher, providing it with fruity, caramel, and sweet aroma (Bi et al., 2021). The ketones detected in samples primarily included 2-butanone, acetone, 2-heptanone, 2-octanone, 3-octan-2-one, and 3-nonen-2-one, which provided the samples with longer-lasting aromas, including grass, cream, and floral ones. The ketones in parched rice were primarily produced by lipid oxidation at high temperatures and the thermal degradation of carbohydrates (Zhang et al., 2020). 2-Ethyl furan is the unique aroma substance in raw proso millet that imparted it with rice malt, bean, and caramel aroma. 2-Methyl tetrahydrofuran is a unique flavor substance in parched rice endowed with fruit and floral aroma. 2-Pentylfuran is a prevalent aromatic substance in roasted food, which brings grass and a sweet aroma to parched rice (Cai et al.,2020). The acids in parched rice (7 in hard parched rice and 4 in crispy parched rice) were higher than that in raw proso millet (5). Acetic, decanoic, hexanoic, and nonanoic acids were detected in raw proso millet and parched rice. After the treatment, the content of hexanoic acid significantly increased, endowing parched rice with a sweet and creamy aroma. Valeric, caprylic, and heptanoic acids were also detected in parched rice. The acid was primarily formed by the oxidation of alcohols and aldehydes, imparting aroma characteristics such as creamy, sour, and fatty aromas to samples (Bi et al., 2021). Hydrocarbons are the by-products of lipid heat breakdown, and hydrocarbons have been found in parched rice. D-Limonene was detected in raw proso millet and parched rice, providing fresh orange and lemon aromas (Zhang et al., 2020).

#### 3.7.2. Analysis of e-nose and volatile compounds

The PEN3 e-nose contained 10 metal-oxide sensors sensitive to different gas concentrations, and their relative conductivity ratio ($G/G_0$) varied with gas concentration (Wu et al., 2021). Fig. 3H exhibits the response of the sensors to volatile substances in the samples. It could be deduced that the $G/G_0$ response intensity of each sensor did not significantly change when various raw proso millets were detected, indicating that the volatile components of various raw proso millets were similar. The volatile component concentration of different kinds of parched rice differed significantly from that of raw proso millet. The relative conductivities of W5S and W1W sensors in parched rice were significantly higher than those in raw proso millet, indicating that nitrogen oxides

and sulfides were the predominant volatile flavoring agents in parched rice. Except for the W5S and W1W sensors, the response signal levels of parched rice in the other sensors did not significantly differ from those of raw proso millet, albeit slightly higher. These results indicated that thermal treatment increased the content of volatile components and provided a richer odor for parched rice.

## 4. Conclusion

This study revealed the effects of steaming, roasting, and milling on the structure, nutrition, and flavor of proso millet. The A-type starch crystal in raw proso millet was destroyed, and the short-range order degree and double-helix structure decreased. The starch in parched rice formed complexes with lipid and protein and exhibited a V-type crystal. Changes in the structure of parched rice endowed it with distinct properties. The decreased viscosity and thermal stability of parched rice paste and its higher digestibility indicated that it was suitable for rapidly generating foods that supplied energy and were easy to digest. Hard parched rice displayed the weakest structural integrity, the lowest gel viscosity and stability, and the highest starch digestibility, considerably influenced by the longer thermal treatment time. Thermal treatment also provided parched rice with richer flavor compounds. Findings in this study can serve as a theoretical basis for proso millet processing and demonstrate the excellent potential of proso millet in industrially processing whole grains. This work comprehensively investigated the effects of thermal treatment on proso millet. However, further studies can be conducted to improve the utilization of proso millet through more cooking methods.

## CRediT authorship contribution statement

**Yulian Zhu:** Conceptualization, Formal analysis, Investigation, Writing – original draft. **Fei Xie:** Conceptualization, Validation, Formal analysis, Visualization. **Jing Ren:** Methodology, Conceptualization, Formal analysis, Visualization. **Fan Jiang:** Formal analysis, Data curation, Writing – review & editing. **Ning Zhao:** Software, Data curation, Writing – review & editing. **Shuang-kui Du:** Funding acquisition, Resources, Supervision, Conceptualization, Methodology, Data curation, Formal analysis, Validation, Supervision, Writing – review & editing.

## Declaration of Competing Interest

The authors declare that they have no known competing financial interests or personal relationships that could have appeared to influence the work reported in this paper.

## Data availability

Data will be made available on request.

## Acknowledgements

The authors would like to thank Key Research and Development Program Project of Shaanxi Province (2021NY-155), Shaanxi Province Agricultural Science and Technology Innovation and Transformation Project (NYKJ-2020-YL19).

## Appendix A. Supplementary data

Supplementary data to this article can be found online at https://doi.org/10.1016/j.fochx.2023.100784.

## References:

AOAC. (2005). *Official Methods of Analysis of AOAC International* (18th edn.). AOAC International, Gaithersberg.

Bi, S., Wang, A., Lao, F., Shen, Q., Liao, X., Zhang, P., & Wu, J. (2021). Effects of frying, roasting and boiling on aroma profiles of adzuki beans (*Vigna angularis*) and potential of adzuki bean and millet flours to improve flavor and sensory characteristics of biscuits. *Food Chemistry, 339*, Article 127878.

Cai, J., Zhu, Y., Ma, R., Thakur, K., Zhang, J., & Wei, Z. (2020). Effects of roasting level on physicochemical, sensory, and volatile profiles of soybeans using electronic nose and HS-SPME-GC-MS. *Food Chemistry, 340*, Article 127880.

Du, C., Jiang, F., Jiang, W., Ge, W., & Du, S. (2020). Physicochemical and structural properties of sago starch. *International Journal of Biological Macromolecules, 164*, 1785–1793.

Duque, S. M. M., Leong, S. Y., Agyei, D., Singh, J., Larsen, N., & Oey, I. (2020). Understanding the impact of Pulsed Electric Fields treatment on the thermal and pasting properties of raw and thermally processed oat flours. *Food Research International, 129*, Article 108839.

Dharmaraj, U., Parameswara, P., Somashekar, R., & Malleshi, N. G. (2014). Effect of processing on the microstructure of finger millet by X-ray diffraction and scanning electron microscopy. *Journal of Food Science & Technology, 51*, 494–502.

Ding, Y., Yang, L., Xia, Y., Wu, Y., Zhou, Y., & Wang, H. (2018). Effects of frying on starch structure and digestibility of glutinous rice cakes. *Journal of Cereal Science, 83*, 196–203.

Gao, S., Zhang, H., Pei, J., Liu, H., Lu, M., Chen, J., & Wang, M. (2022). High-voltage and short-time dielectric barrier discharge plasma treatment affects structural and digestive properties of *Tartary* buckwheat starch. *International Journal of Biological Macromolecules., 213*, 268–278.

Gulati, P., Li, A., Holding, D., Santra, D., Zhang, Y., & Rose, D. J. (2017). Heating reduces proso millet protein digestibility via formation of hydrophobic aggregates. *Journal of Agricultural and Food Chemistry, 65*, 1952–1959.

Huong, N. T. M., Hoa, P. N., & Hung, P. V. (2021). Effects of microwave treatments and retrogradation on molecular crystalline structure and in vitro digestibility of debranched mung-bean starches. *International Journal of Biological Macromolecules, 190*, 904–910.

Heiniö, R. L., Noort, M. W. J., Katina, K., Alam, S. A., Sozer, N., de Kock, H. L., … Poutanen, K. (2016). Sensory characteristics of wholegrain and bran-rich cereal foods – A review. *Trends in Food Science & Technology, 47*, 25–38.

Jiang, F., Du, C., Guo, Y., Fu, J., Jiang, W., & Du, S. K. (2020). Physicochemical and structural properties of starches isolated from quinoa varieties. *Food Hydrocolloids, 101*, Article 105515.

Jiang, F., Du, C., Zhao, N., Jiang, W., Yu, X., & Du, S. (2022). Preparation and characterization of quinoa starch nanoparticles as quercetin carriers. *Food Chemistry, 369*, Article 130895.

Kumar, S. R., Sadiq, M. B., & Anal, A. K. (2020). Comparative study of physicochemical and functional properties of pan and microwave cooked underutilized millets (proso and little). *LWT, 128*, Article 109465.

Li, W., Wen, L., Chen, Z., Zhang, Z., & Guo, Y. (2021). Study on metabolic variation in whole grains of four proso millet varieties reveals metabolites important for antioxidant properties and quality traits. *Food Chemistry, 357*(4), Article 129791.

Liu, J., Tang, X., & Zhang, Y. (2012). Determination of the volatile composition in brown millet, milled millet and millet bran by gas chromatography/mass spectrometry. *Molecules, 17*, 2271–2282.

Lina, G., & Min, Z. (2022). Formation and release of cooked rice aroma. *Journal of Cereal Science, 107*, Article 103523.

Long, G., Ji, Y., Pan, H., Sun, Z., Li, Y., & Qin, G. (2015). Characterization of thermal denaturation structure and morphology of soy glycinin by FTIR and SEM. *International Journal of Food Properties, 18*(4), 763–774.

Lu, X., Xu, R., Zhan, J., Chen, L., Jin, Z., & Tian, Y. (2020). Pasting, rheology, and fine structure of starch for waxy rice powder with high-temperature baking. *International Journal of Biological Macromolecules, 146*, 620–626.

Ma, Q., Zhao, Y., Wang, H. L., Li, J., Yang, Q., Gao, L., … Feng, B. (2020). Comparative study on the effects of buckwheat by roasting: Antioxidant properties, nutrients, pasting, and thermal properties. *Journal of Cereal Science, 95*, Article 103041.

Marti, A., & Tyl, C. (2021). Capitalizing on a double crop: Recent advances in proso millet's transition to a food crop. *Comprehensive Reviews in Food Science and Food Safety, 20*, 819–839.

McSweeney, M. B., Seetharaman, K., Ramdath, D. D., & Duizer, L. M. (2017). Chemical and physical characteristics of proso millet (*Panicum miliaceum*)-based products. *Cereal Chemistry Journal, 94*, 357–362.

Olamiti, G., Takalani, T. K., Beswa, D., & Jideani, A. I. O. (2020). Effect of malting and fermentation on colour, thermal properties, functional groups and crystallinity level of flours from pearl millet (*Pennisetum glaucum*) and sorghum (*Sorghum bicolor*). *Heliyon, 6*(12), e05467.

Qian, X., Sun, B., Zhu, C., Zhang, Z., Tian, X., & Wang, X. (2020). Effect of stir-frying on oat milling and pasting properties and rheological properties of oat flour. *Journal of Cereal Science, 92*, Article 102908.

Solaesa, Á. G., Villanueva, M., Vela, A. J., & Ronda, F. (2022). Impact of microwave radiation on in vitro starch digestibility, structural and thermal properties of rice flour. From dry to wet treatments. *International Journal of Biological Macromolecules, 222*, 1768–1777.

Saleh, A. S. M., Zhang, Q., Chen, J., & Shen, Q. (2013). Millet grains: Nutritional quality, processing, and potential health benefits. *Comprehensive Reviews in Food Science and Food Safety, 12*, 281–295.

Srikaeo, K., Furst, J., Hosken, R., & Ashton, J. (2005). Physical properties of cooked wheat grains as affected by cooking temperature and duration. *International Journal of Food Properties, 8*, 469–479.

Starr, G., Bredie, W. L. P., & Hansen, Å. S. (2013). Sensory profiles of cooked grains from wheat species and varieties. *Journal of Cereal Science, 57*(3), 295–303.

Sun, Q., Gong, M., Li, Y., & Xiong, L. (2014). Effect of dry heat treatment on the physicochemical properties and structure of proso millet flour and starch. *Carbohydrate. Polymers, 110*, 128–134.

Vinutha, T., Kumar, D., Bansal, N., Krishnan, V., Goswami, S., Kumar, R. R., … Praveen, S. (2022). Thermal treatments reduce rancidity and modulate structural and digestive properties of starch in pearl millet flour. *International Journal of Biological Macromolecules, 195*, 207–216.

Wani, I. A., Hamid, H., Hamdani, A. M., Gani, A., & Ashwar, B. A. (2017). Physico-chemical, rheological and antioxidant properties of sweet chestnut (*Castanea sativa Mill.*) as affected by pan and microwave roasting. *Journal of Advanced Research, 8*, 399–405.

Wang, Z., Zhong, Z., Zheng, B., Zhang, Y., & Zeng, H. (2023). Effects of *Porphyra haitanensis* polysaccharides on gelatinization and gelatinization kinetics of starches with different crystal types. *International Journal of Biological Macromolecules, 242*(Pt 3), Article 125117.

Wu, J., Ling, C., Chen, Y., Li, Z., Song, F., Raghavan, G. S. V., … Song, C. (2021). Monitoring and control of microwave drying with volatiles detection of celery stalks. *Computers and Electronics in Agriculture, 187*, 106256.

Yang, Q., Zhang, P., Qu, Y., Gao, X., Liang, J., Yang, P., & Feng, B. (2018). Comparison of physicochemical properties and cooking edibility of waxy and non-waxy proso millet (*Panicum miliaceum* L.). *Food Chemistry, 257*, 271–278.

Yang, Z., Hao, H., Wu, Y., Liu, Y., & Ouyang, J. (2021). Influence of moisture and amylose on the physicochemical properties of rice starch during heat treatment. *International Journal of Biological Macromolecules, 168*, 656–662.

Zhang, Y., Tang, N., Shi, L., Miao, Y., Liu, X., Ge, X., … Zhang, X. (2020). Characterization and comparison of predominant aroma compounds in microwave-treated wheat germ and evaluation of microwave radiation on stability. *Journal of Cereal Science, 93*, Article 102942.

Zhao, S., Jiao, A., Yang, Y., Liu, Q., & Jin, Z. (2021). Modification of physicochemical properties and degradation of barley flour upon enzymatic extrusion. *Food Bioscience, 45*, Article 101243.